

Ion Trap/Ion Mobility/Quadrupole/Time-of-Flight Mass Spectrometry for Peptide Mixture Analysis

Cherokee S. Hoaglund-Hyzer and David E. Clemmer*

Department of Chemistry, Indiana University, Bloomington IN, 47405

An ion trap/ion mobility/quadrupole/time-of-flight mass spectrometer has been developed for the analysis of peptide mixtures. In this approach, a mixture of peptides is electrosprayed into the gas phase. The mixture of ions that is created is accumulated in an ion trap and periodically injected into a drift tube where ions separate according to differences in gas-phase ion mobilities. Upon exiting the drift tube, ions enter a quadrupole mass filter where a specific mass-to-charge (m/z) ratio can be selected prior to collisional activation in an octopole collision cell. Parent and fragment ions that exit the collision cell are analyzed using a reflectron geometry time-of-flight mass spectrometer. The overall configuration allows different species to be selected according to their mobilities and m/z ratios prior to collision-induced dissociation and final MS analysis. A key parameter in these studies is the pressure of the target gas in the collision cell. Above a critical pressure, the well-defined mobility separation degrades. The approach is demonstrated by examining a mixture of tryptic digest peptides of ubiquitin.

The combination of liquid chromatography (LC) with electrospray ionization (ESI)¹ mass spectrometry (MS) is currently receiving considerable attention for the analysis of complex biological samples. The incorporation of multiple stages of MS (MS/MS) provides direct information about sequence,² especially when coupled with database search algorithms.³ A particularly important LC-MS/MS configuration involves the combination of quadrupole (Q) and time-of-flight (TOF) mass spectrometers. In this configuration, the initial mass filter is used to select a narrow m/z range, and all fragments formed by collision-induced dissociation (CID) are analyzed by the TOF mass spectrometer. The dispersive nature of the TOF analysis, compared to the scanning Q analysis, improves sensitivity and allows rapid acquisition of complete fragmentation mass spectra.

In this paper we describe the initial development of a related technique, the combination of ion mobility spectrometry (IMS)

with a Q/TOF spectrometer. We have previously reported an IMS-TOF approach,⁴ substantial differences in the time scale required for each separation (milliseconds in the high-pressure drift tube, compared to microseconds in the evacuated TOF instrument) allow mobilities and m/z ratios for mixtures of ions to be acquired in a single experimental sequence. An illustration of a hypothetical IMS-TOF dataset showing the two-dimensional analysis of a mixture of ions is shown in Figure 1. The hybrid approach offers advantages in resolving components of complex samples,⁵ especially isomers, as illustrated in several recent studies of combinatorial peptide libraries.^{6,7} Recently, we developed a configuration that utilizes a gas cell between the IMS and TOF instruments.⁸ Fragments of mobility-separated ions occur at drift times that are coincident with their antecedent parents. Figure 1 also shows an illustration of this approach. Here, fragments generated from a mixture of ions have drift times that are coincident with their antecedent precursors, in effect, tagging fragments and parents such that a mixture can be analyzed in a parallel fashion. The hypothetical dataset (Figure 1) illustrates a parallel CID experiment that is complicated by the fact that two precursor ions have identical mobilities. In this case, the fragments that are formed (for components 3 and 4) cannot be ascribed to a unique precursor. In this paper, we provide the first illustration of a method that can overcome this limitation, an IMS-Q/TOF approach. The initial mass filter can be invoked when multiple ions in the mixture have overlapping drift times. As illustrated in Figure 1, the combination of mobility and m/z selection allows fragments to be unambiguously assigned to a specific m/z -selected parent ion, even when two ions have identical mobilities. Below, we demonstrate the IMS-Q/TOF approach by analyzing a mixture of peptides from a tryptic digest of ubiquitin. The results show that a key parameter in these studies is the dissociation time scale. If the target gas pressure is above a critical level, ion scattering in the cell degrades the temporal resolution of the mobility separation. This is explored by examining bradykinin, a system that has been characterized extensively.^{9,10}

(1) Fenn, J. B.; Mann, M.; Meng, C. K.; Wong, S. F.; Whitehouse, C. M. *Science* **1989**, *246*, 64.

(2) Papayannopoulos, I. A. *Mass Spectrom. Rev.* **1995**, *14*, 49.

(3) For recent discussions of protein databases and search algorithms, see the following and references therein: (a) Eng, J. K.; McCormack, A. L.; Yates, J. R., III *J. Am. Soc. Mass Spectrom.* **1994**, *5*, 976. (b) Yates, J. R., III.; Eng, J. K.; Clauser, K. R.; Burlingame, A. L. *J. Am. Soc. Mass Spectrom.* **1996**, *7*, 1089. (c) Jensen, O. N.; Podtelejnikov, A. V.; Mann, M. *Anal. Chem.* **1997**, *69*, 4741. (d) Reiber, D. C.; Grover, T. A.; Brown, R. S. *Anal. Chem.* **1998**, *70*, 673. (e) Yates III, J. R. *Electrophoresis* **1998**, *19*, 893. (f) Clauser, K. R.; Baker, P.; Burlingame, A. L. *Anal. Chem.* **1999**, *71*, 2871.

(4) Hoaglund, C. S.; Valentine, S. J.; Sporleder, C. R.; Reilly, J. P.; Clemmer, D. E. *Anal. Chem.* **1998**, *70*, 2236.

(5) Henderson, S. C.; Valentine, S. J.; Counterman, A. E.; Clemmer, D. E. *Anal. Chem.* **1999**, *71*, 291.

(6) Srebalus, C. A.; Li, J.; Marshall, W. S.; Clemmer, D. E. *Anal. Chem.* **1999**, *71*, 3918.

(7) Srebalus, C. A.; Li, J.; Marshall, W. S.; Clemmer, D. E. *J. Am. Soc. Mass Spectrom.* **2000**, *11*, 352.

(8) Hoaglund-Hyzer, C. S.; Li, J.; Clemmer, D. E. *Anal. Chem.* **2000**, *72*, 2737.

(9) Wyttenbach, T.; von Helden, G.; Bowers, M. T. *J. Am. Chem. Soc.* **1996**, *118*, 8355.

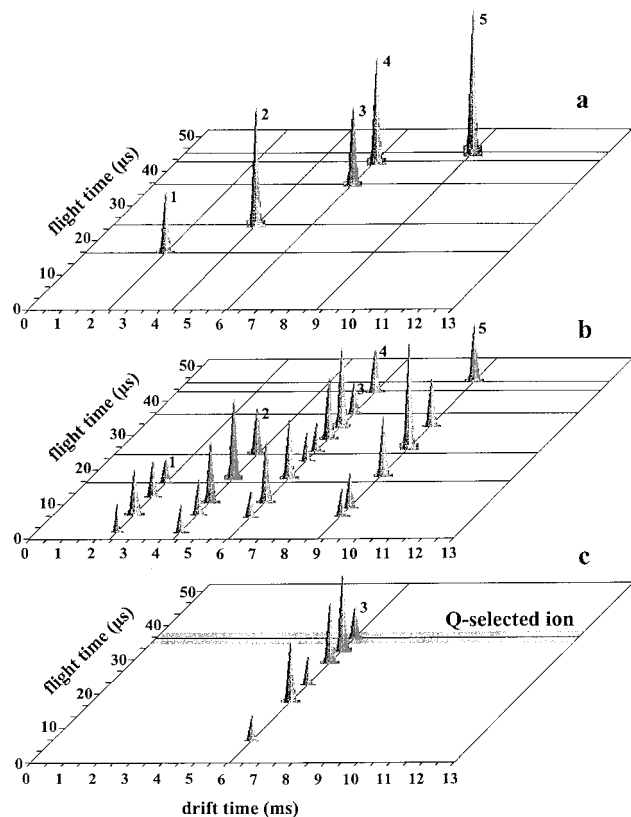


Figure 1. This plot shows three hypothetical datasets illustrating several IMS-MS configurations. Part a shows an IMS-TOF analysis of a mixture containing five components. Note that two of the components (labeled 3 and 4) have identical mobilities but different m/z ratios. Part b shows an IMS-TOF analysis of the same mixture when a collision cell has been introduced between the mobility and TOF instruments. This experimental configuration is analogous to the one that is described in ref 8. Under these conditions, precursor ions are separated by differences in their mobilities and then injected into the collision cell. Fragment ions that are produced in the collision cell are coincident with their antecedent parents. This configuration allows components 1, 2, and 5 to be sequenced in parallel. Fragments from components 3 and 4 are also apparent, but unambiguous assignment of fragments to precursors is not possible because the mobilities of these ions are identical. Part c shows the hypothetical dataset that is obtained using the IMS-Q/TOF configuration. Here, the quadrupole has been used to select component 3, which allows the origin of fragment peaks to be unambiguously assigned.

Ion mobility techniques¹¹ have traditionally been used to detect small analytes,¹² (e.g., explosives, chemical warfare agents) and for particle sizing.^{13,14} The mobility of an ion through a buffer gas depends on the shape of the ion, and the recent combination of mobility measurements with theoretical models for calculating

mobility¹⁵ has led to what is effectively a new form of spectroscopy that provides information about the geometries of clusters,¹⁶ synthetic polymers,¹⁷ and biomolecular ions.^{10,18–27} Although the combination of mobility measurements and calculations cannot provide detailed atomic information, this approach is currently the most direct means of assessing the shapes of ions containing more than a handful of atoms. Linear regression analysis of the mobilities for large numbers of peptides has provided intrinsic size parameters for individual amino acid residues.^{20,26} These size parameters can be combined with sequences to provide an additional constraint for identifying individual peptides in large mixtures.²⁸ A number of IMS-MS configurations currently exist, including several high- and low-resolution IMS-Q and Q-IMS-Q [including an ion trap (IT) in the front of the drift tube]^{29,30} and IMS-TOF^{5,31} and IT-IMS-TOF.⁵ Recently, ESI^{32,33} and laser desorption ion sources^{34–36} have been coupled to most of these configurations.

(10) Counterman, A. E.; Valentine, S. J.; Srebalus, C. A.; Henderson, S. C.; Hoaglund, C. S.; Clemmer, D. E. *J. Am. Soc. Mass Spectrom.* **1998**, *9*, 743.
 (11) See, for example: (a) Tou, J. C.; Boggs, G. U. *Anal. Chem.* **1976**, *48*, 351. (b) Hagen, D. F. *Anal. Chem.* **1979**, *51*, 870. (c) Hill, H. H.; Siems, W. F.; St. Louis, R. H.; McMinn, D. G.; *Anal. Chem.* **1990**, *62*, 1201A. (d) St. Louis, R. H.; Hill, H. H. *Crit. Rev. Anal. Chem.* **1990**, *21*, 321. (e) von Helden, G.; Hsu, M.-T.; Kemper, P. R.; Bowers, M. T. *J. Chem. Phys.* **1991**, *95*, 3835. (f) Jarrold, M. F. *J. Phys. Chem.* **1995**, *99*, 11. (g) Clemmer, D. E.; Jarrold, M. F. *J. Mass Spectrom.* **1997**, *32*, 577.
 (12) Karpas, Z.; Stimac, R. M.; Rappaport, Z. *Int. J. Mass Spectrom. Ion Processes* **1988**, *83*, 163.
 (13) Whitby, K. T.; Clark, W. E. *Tellus* **1966**, *18*, 573.
 (14) Sanders, T. M.; Forest, S. R. *J. Appl. Phys.* **1989**, *66*, 3317.

(15) See, for example: (a) Jarrold, M. F.; Constant, V. A. *Phys. Rev. Lett.* **1991**, *67*, 2994. (b) Wyttenbach, T.; von Helden, G.; Batka, J. J., Jr.; Carlat, D.; Bowers, M. T. *J. Am. Soc. Mass Spectrom.* **1997**, *8*, 275. (c) Mesleh, M. F.; Hunter, J. M.; Shvartsburg, A. A.; Schatz, G. C.; Jarrold, M. F. *J. Phys. Chem.* **1996**, *100*, 16082. (d) Shvartsburg, A. A.; Jarrold, M. F. *Chem. Phys. Lett.* **1996**, *261*, 86.
 (16) Jarrold, M. F.; Bower, J. E.; Creegan, K. J. *Chem. Phys.* **1989**, *90*, 3615.
 (17) See, for example: (a) von Helden, G.; Wyttenbach, T.; Bowers, M. T. *Science*, **1995**, *267*, 1483. (b) von Helden, G.; Wyttenbach, T.; Bowers, M. T. *Int. J. Mass Spectrom. Ion Processes* **1995**, *146/147*, 349. (c) Wyttenbach, T.; von Helden, G.; Bowers, M. T. *Int. J. Mass Spectrom. Ion Processes* **1997**, *165/166*, 377. (d) Gidden, J.; Wyttenbach, T.; Batka, J. J.; Weis, P.; Jackson, A. T.; Scrivens, J. H.; Bowers, M. T. *J. Am. Chem. Soc.* **1999**, *121*, 1421. (e) Gidden, J.; Wyttenbach, T.; Batka, J. J.; Weis, P.; Jackson, A. T.; Scrivens, J. H.; Bowers, M. T. *J. Am. Soc. Mass Spectrom.* **1999**, *10*, 883.
 (18) (a) Wyttenbach, T.; von Helden, G.; Bowers, M. T. *J. Am. Chem. Soc.* **1996**, *118*, 8355. (b) Wyttenbach, T.; Bushnell, J. E.; Bowers, M. T. *J. Am. Chem. Soc.* **1998**, *120*, 5098.
 (19) Clemmer, D. E.; Hudgins, R. R.; Jarrold, M. F. *J. Am. Chem. Soc.* **1995**, *117*, 10141. Shelimov, K. B.; Clemmer, D. E.; Hudgins, R. R.; Jarrold, M. F. *J. Am. Chem. Soc.* **1997**, *119*, 2240. Hudgins, R. R.; Ratner, M. A.; Jarrold, M. F. *J. Am. Chem. Soc.* **1998**, *120*, 12974. Hudgins, R. R.; Mao, Y.; Ratner, M. A.; Jarrold, M. F. *Biophys. J.* **1999**, *76*, 1591.
 (20) Henderson, S. C.; Li, J.; Counterman, A. E.; Clemmer, D. E. *J. Phys. Chem. B* **1999**, *103*, 8780.
 (21) Counterman, A. E.; Clemmer, D. E. *J. Am. Chem. Soc.*, submitted.
 (22) Valentine, S. J.; Clemmer, D. E. *J. Am. Chem. Soc.* **1997**, *119*, 3558.
 (23) Valentine, S. J.; Anderson, J.; Ellington, A. E.; Clemmer, D. E. *J. Phys. Chem. B* **1997**, *101*, 3891.
 (24) Valentine, S. J.; Counterman, A. E.; Clemmer, D. E. *J. Am. Soc. Mass Spectrom.* **1997**, *8*, 954.
 (25) Hoaglund, C. S.; Liu, Y.; Pagel, M.; Ellington, A. D.; Clemmer, D. E. *J. Am. Chem. Soc.* **1997**, *119*, 9051.
 (26) Valentine, S. J.; Counterman, A. E.; Hoaglund-Hyzer, C. S.; Clemmer, D. E. *J. Phys. Chem.* **1999**, *103*, 1203.
 (27) Hoaglund-Hyzer, C. S.; Counterman, A. E.; Clemmer, D. E. *Chem. Rev.* **1999**, *99*, 3037.
 (28) Valentine, S. J.; Counterman, A. E.; Clemmer, D. E. *J. Am. Soc. Mass Spectrom.* **1999**, *10*, 1188.
 (29) Hoaglund, C. S.; Valentine, S. J.; Clemmer, D. E. *Anal. Chem.* **1997**, *69*, 4156.
 (30) Creaser, C. S.; Benyazzar, M.; Griffiths, J. R.; Stygall, J. W. *Anal. Chem.* **2000**, *72*, 2724.
 (31) Guevremont, R.; Siu, K. W. M.; Wang, J.; Ding, L. *Anal. Chem.* **1997**, *69*, 3959.
 (32) Wittmer, D.; Chen, T. H.; Luckenbill, B. K.; Hill, H. H. *Anal. Chem.* **1994**, *66*, 2348.
 (33) Clemmer, D. E.; Hudgins, R. R.; Jarrold, M. F. *J. Am. Chem. Soc.* **1995**, *117*, 10141.
 (34) von Helden, G.; Kemper, P. R.; Gotts, N. G.; Bowers, M. T. *Science* **1993**, *259*, 1300.
 (35) Shelimov, K. B.; Hunter, J. M.; Jarrold, M. F. *Int. J. Mass Spectrom. Ion Processes* **1994**, *138*, 17.
 (36) Russell, D. H.; Gillig, K. J.; Stone, E.; Park, Z.-Y.; Fuhrer, K.; Gonin, M. Schultz, A. J. *Proc. SPIE* **2000**, *3926*, 69.

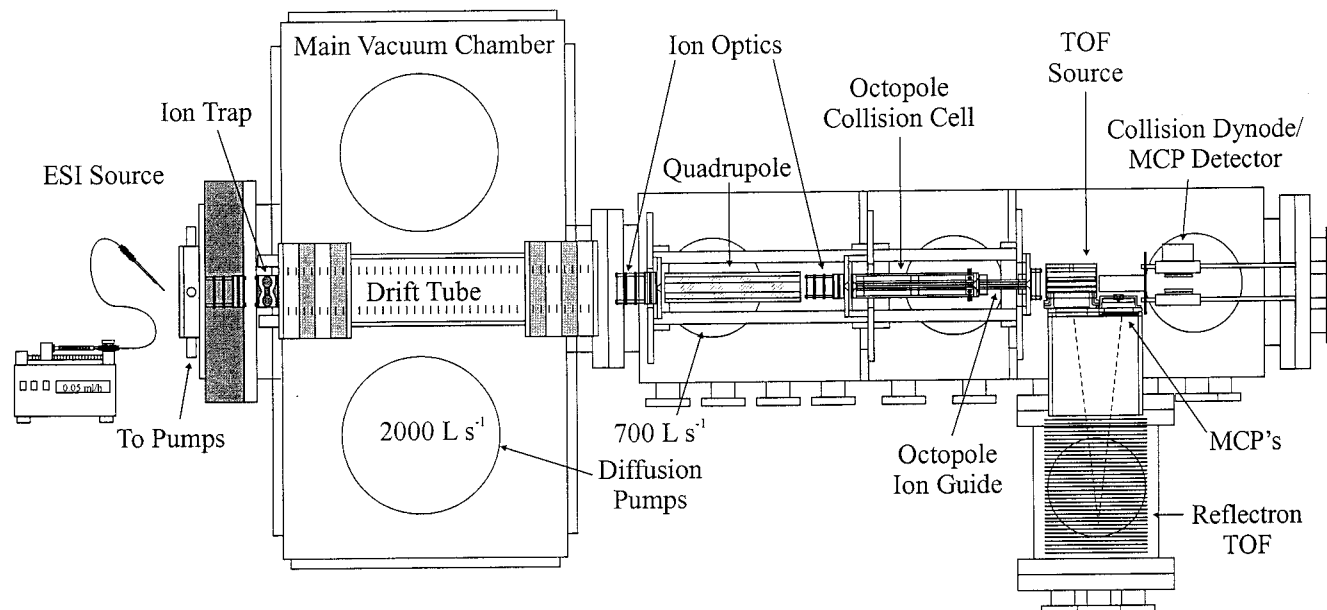


Figure 2. Schematic diagram of the ESI/ion trap/drift tube/quadrupole/collision cell/reflection time-of-flight mass spectrometer. The apparatus is described in detail in the text.

EXPERIMENTAL SECTION

General. A schematic diagram of the experimental apparatus is shown in Figure 2. There are six primary components, including (1) an ESI source, (2) a quadrupole ion trap, (3) an injected-ion drift tube, (4) a quadrupole mass filter, (5) an octopole collision cell, and (6) a TOF mass spectrometer. Each component is described in detail below. A brief description of a typical experimental sequence is as follows. The continuous beam of electrosprayed ions is extracted into a high-vacuum region and accumulated in the quadrupole ion trap. Experiments are initiated by injecting a short pulse of ions into the drift tube containing He buffer gas. Ions drift through the gas under the influence of a weak uniform electric field and are separated due to differences in their mobilities through the gas. The drift force experienced by the ions is proportional to the charge state such that high-charge state ions have higher mobilities than low-charge state ions. For tryptic peptides, we often observe families of ions corresponding to $[M + H]^+$, $[M + 2H]^{2+}$, and sometimes $[M + 3H]^{3+}$ ions.³⁷ Within a charge-state family, ions with compact geometries have higher mobilities than those with more open structures. Ions that exit the drift tube are focused into a quadrupole mass filter that can be set to transmit all ions or to select specific m/z species. As ions exit the quadrupole, they are decelerated to a desired kinetic energy and injected into an octopole collision cell. For CID studies, the collision cell is filled with a target gas (usually UHP zero-grade argon, Air Products). Parents and fragments exit the gas cell into a second octopole that guides ions into the source region of a reflectron geometry TOF mass spectrometer where flight times are measured.

Sample Preparation and Ion Formation. Ubiquitin digests were prepared by a procedure that is similar to one outlined previously.³⁸ A 20 mg mL⁻¹ solution of ubiquitin (Sigma, bovine 90%) in 0.2 M ammonium bicarbonate (EM Science) was incu-

bated at 90° for ~20 min in order to thermally denature the protein. The denatured state was quenched by rapidly cooling the solution to 0 °C in an ice water bath. This solution was then combined with a 0.2 mg mL⁻¹ trypsin (Sigma, bovine) solution in 0.2 M ammonium bicarbonate (in ~50-fold excess protein, by weight) and incubated for 20 h at 37 °C. The trypsin was filtered from the digest using a microconcentrator (microcon 10, Amicon) and the peptides that remained were lyophilized.³⁹

Solutions containing 1.0 mg mL⁻¹ of the lyophilized peptide mixture in 49:49:2 (% volume) water:acetonitrile:acetic acid were electrosprayed at atmospheric pressure into a 5.0-cm-long differentially pumped desolvation region operated at a pressure of ~1 to 10 Torr. Some of the ions exit the differentially pumped cavity through a 0.012-cm diameter orifice and enter the main vacuum chamber. This chamber is pumped by two ISO-250 diffusion pumps (Edwards, 2000 L sec⁻¹), and the background pressure in this region during experiments is typically 10⁻⁵ to 10⁻⁴ Torr.

Ion Accumulation and Mobility Separation. Ions from the source are focused into a low-energy beam and guided into an ion trap (R. M. Jordan, model C-1251). The ion trap consists of a center ring (operated at 1.1 MHz and ~2600 V_{pp}) and two end caps that are mounted directly to the entrance plate of the drift tube. The trap contains ~10⁻⁴ to 10⁻³ Torr of He buffer gas that is supplied from buffer gas that leaks out of the entrance of the drift tube (as well as ambient background gas from the main chamber).²⁹

Ions are ejected from the trap into the drift tube by turning the rf field off and supplying a short dc pulse (0.6 μs) to one of the end caps. An important parameter is the voltage used to inject ions into the drift tube. In these studies, injection voltages from 60 to 150 V were used. As ions enter the drift tube they undergo a rapid heating/cooling cycle.^{40,41} Initial collisions with the buffer gas thermalize the kinetic energy of the ions and excite internal degrees of freedom; further collisions cool ion internal energies

(37) Valentine, S. J.; Counterman, A. E.; Hoaglund, C. S.; Reilly, J. P.; Clemmer, D. E. *J. Am. Soc. Mass Spectrom.* **1998**, *9*, 1213.

(38) Park, Z.-Y.; Russell, D. H. *Anal. Chem.* **2000**, *72*, 2667.

(39) For a detailed discussion, see: *Protein Sequencing: A Practical Approach*; Findlay, J. B. C.; Gelsow, M. J., Eds.; IRL: Oxford, 1989; p 43.

to the temperature of the buffer gas (300 K). For peptides containing ~8 to 16 residues, $[M + 2H]^{2+}$ ions are favored at low injection voltages. At higher injection voltages (≥ 100 V), doubly charged ions often undergo an endothermic proton-transfer reaction (i.e., $[M + 2H]^{2+} \rightarrow [M + H]^+ + HeH^+$), which favors singly protonated peptides.⁴² These higher injection voltages also promote fragmentation of peptides at the front of the drift tube.^{29,43} In some cases, we observe multiply charged multimers at low injection voltages; at higher injection voltages these often dissociate to produce singly charged monomers.

The drift tube is 53.3 cm long with 0.016-cm diameter entrance and exit apertures. The body is made of a stainless steel tube and several copper spacers. Entrance and exit plates are electrically isolated from the drift tube body by ceramic spacers. A uniform field along the drift axis is created by 42 equally spaced 0.025-cm-thick BeCu rings that are connected in series by 5.00 M Ω high-vacuum resistors (Victoreen, $\pm 1\%$). Data were recorded using ~2 to 3 Torr of 300 K He buffer gas and applied drift fields of 10–12 V cm⁻¹.

Quadrupole, Collision Cell, and TOF Regions. Ions that exit the drift tube are focused into the detector chamber that is segmented into four sections. Each is pumped by an ISO-160 diffusion pump (Edwards, 700 L s⁻¹). The first section houses an Extrel quadrupole mass spectrometer. Typically the pressure in this section during experiments is $\sim 10^{-5}$ Torr. The quadrupole can be operated in rf-only mode in order to pass all ions or the system can be used to pass a selected m/z window over a ~10 to 4000 u range.

As ions exit the quadrupole, they are decelerated to a desired kinetic energy and focused into the second section that contains the octopole collision cell. The collision cell body is made from a 19.1-cm-long stainless steel tube having a 3.81-cm i.d. Ions enter and exit the cell through 0.635-cm-diam holes centered on electrically isolated endcaps. Eight stainless steel rods (0.318-cm diam) that are 19.1 cm long are situated in three macor mounts that center the rods on a 1.270-cm-diam circle inside the collision cell body. A port in the collision cell case allows target gases to be added to the cell; pressures in the cell are controlled by a leak valve (Granville Phillips, model 203) and monitored by a capacitance manometer (MKS, model 640A, Baratron) that is connected to a second port in the collision cell case. The pressure of the collision cell during CID experiments is typically maintained from ~1 to 4×10^{-4} Torr.

Ions that exit the collision cell are transmitted through a second 7.62-cm-long octopole ion guide that is maintained at the background pressure of the octopole section of the chamber (~20 times below the collision cell pressure). In the studies presented below, a dc bias is applied to the rods of the collision cell (-10 to -30 V) and to the ion guide (-40 to -60 V). Rf potentials, opposite

in phase for adjacent rods (2.2 MHz, 826.4 V_{pp}), were applied to both sets of rods.

Upon exiting the second octopole, ions are focused between a pulsing plate and an extraction grid (Ni mesh, Buckbee-Mears, 90% transmittance) associated with the source region of a reflectron geometry TOF mass spectrometer. The primary ion beam can be transmitted through this region and focused onto an off-axis collision dynode/dual-microchannel plate detector. This detector allows a number of experiments to be performed. First, on-axis detection allows all instrumental parameters to be varied in order to optimize the ion signal. Second, the quadrupole mass spectrometer can be scanned in order to record the m/z ratios of the ions that are present. Finally, ion mobility distributions can be collected for all of the ions (by operating the quadrupole in the rf-only mode) or for specific m/z ions.

The orthogonal TOF mass spectrometer can be activated by applying high-frequency (10⁴ Hz), high-voltage (500–2000 V) pulses to the back plate of a two-stage TOF source. Pulses (0.5–3.0 μ s) are supplied by a Directed Energy Inc., model GRX-3.OK-H pulser. The final source grid establishes the flight tube potential (7 kV in most experiments); the configuration results in a 17.5-cm-long field-free region. A grid at the back of the flight tube defines an electrostatic mirror that is generated by applying a uniform retarding potential field to 20 stainless steel rings. Reflected ions are detected by a pair of microchannel plates (Galileo). The resolution ($m/\Delta m$ where Δm is defined as the full width at half-maximum of the peak) of the TOF instrument is typically 500–1200.

Acquisition of Ion Mobility/Time-of-Flight Data. The difference in time scales of ion drift times (t_D) and ion flight times (t_F) allows flight-time distributions to be recorded within individual time windows of the ion mobility spectrum. We refer to this as a nested drift(flight) time measurement. Unless otherwise stated, values of $t_D(t_F)$ are reported as ms(μ s). The acquisition method has been described in detail elsewhere.⁴ Briefly, the initial injection pulse activates a programmable delay generator (PDG) that triggers the high-voltage TOF pulser at specified delay times. Flight times in the mass spectrometer were recorded using a time-to-digital converter (TDC) that is also initiated by the PDG pulse sequence. The TDC records the time that ions reach the detector and can store 128 events during each TOF pulse sequence. The instrumental electronics and data acquisition system, including the initial injection pulse, PDG pulse sequence, TDC, and high-voltage TOF pulser were synchronized by an interface and controlled by a Pentium computer.

It is often useful to derive mobilities (or collision cross sections) from the nested datasets. The raw measurement of ions at the detector will include the time required for ions to drift through the mobility instrument and travel through the interface between the drift tube and the TOF mass spectrometer as well as the flight times of ions. In the case of CID studies, the time required to traverse the interface depends on the experimental conditions. The corrections required at high collision cell pressures ($\geq 5 \times 10^{-4}$ Torr) can be substantial and are not well-defined; we generally do not attempt to determine mobilities from measurements for which substantial corrections are required due to residence times in the collision cell. This is explored in more detail below. Unless otherwise stated, values of t_D have been

(40) Measurements of drift times as a function of injection voltage show that under the present experimental conditions, this heating-cooling process must be largely complete during the first few millimeters of the drift tube.

(41) Jarrold, M. F.; Honea, E. C. *J. Phys. Chem.* **1991**, *95*, 9181.

(42) Previous studies of bradykinin in our ion mobility/TOF instrument indicate that at high injection energies, the doubly charged $[M + 2H]^{2+}$ are converted to $[M + H]^+$ via an endothermic proton-transfer process that forms HeH⁺. The proton affinity of He is 42.5 kcal mol⁻¹ (see: Lias, S. G.; Liebman, J. F.; Levin, R. D. *J. Phys. Chem. Ref. Data* **1984**, *13*, 695).

(43) Liu, Y.; Clemmer, D. E. *Anal. Chem.* **1997**, *69*, 2504.

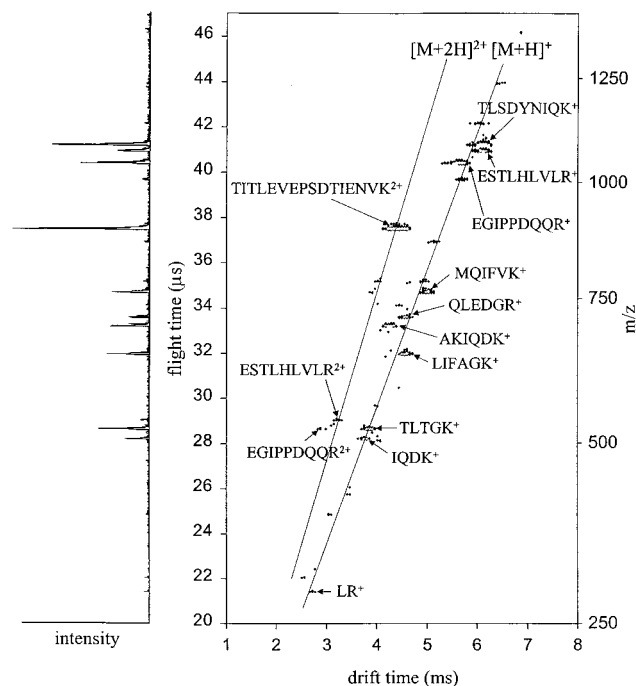


Figure 3. Nested drift(flight) time distribution for an electrosprayed mixture of tryptic peptides of ubiquitin. The flight time axis has been scaled using a standard multipoint calibration of a known ion system. The octopole collision cell was evacuated during the collection of these data, and the quadrupole was set to transmit all ions. Peak labels correspond to sequences that are in agreement with the experimental results expected from the tryptic digestion. The solid lines provide visual guides corresponding to the $[M + H]^+$ and $[M + 2H]^{2+}$ charge state families. The TOF mass spectrum shown on the left was obtained by integrating the two-dimensional data over all drift times. See text for details.

corrected such that it is possible to derive experimental mobilities from them.

RESULTS AND DISCUSSION

Nested Drift(Flight) Time Distribution for All Ions. Figure 3 shows a nested drift(flight) time distribution for a mixture of tryptic peptides obtained from ubiquitin. These data are recorded by setting the quadrupole to pass all ions with the octopole collision cell evacuated to a base pressure of 3×10^{-7} Torr. The plot is similar in appearance to datasets that we have published previously for this system,^{5,37} peaks fall into two primary families according to their charge states ($[M + H]^+$ and $[M + 2H]^{2+}$). We previously discussed the analytical advantages of this separation as well as the origin of slight variations in mobility that occurs within a charge state family.³⁷ Overall, comparisons of experimental masses to calculated values for expected tryptic peptides allow us to assign 10 peaks in the $[M + H]^+$ family; only three of the five peaks observed in the $[M + 2H]^{2+}$ family can be assigned to tryptic fragments (see Figure 3 for assignments). The assignments in the $[M + H]^+$ family include one peak at 4.28(33.20, $m/z = 702.3$)⁴⁴ that is attributed to AKIQDK, a peptide that arises from incomplete digestion.

(44) Flight times for peaks were converted to m/z ratios using a standard calibration. Assignments were made by comparison of experimental m/z ratios with values from the MSProduct program from Protein Prospector <http://prospector.ucsf.edu>.

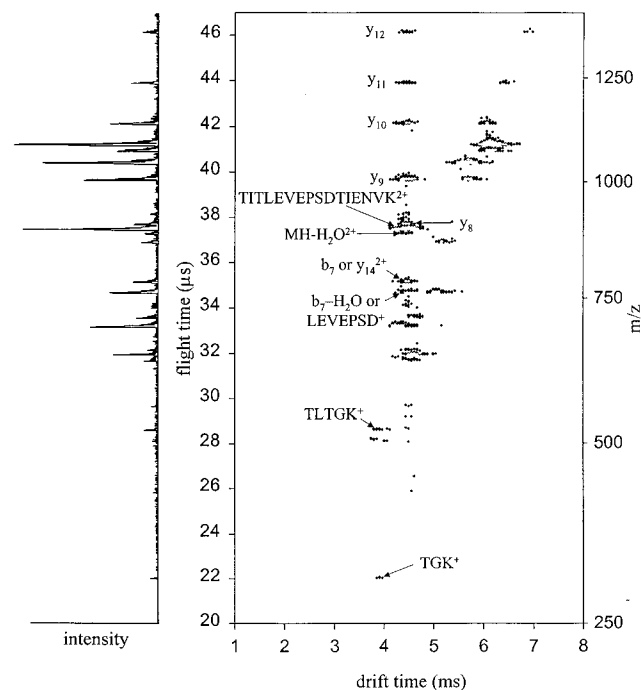


Figure 4. Nested drift(flight) time distribution for the same ubiquitin tryptic mixture as in Figure 3. For these data, 3.8×10^{-4} Torr of argon was added to the octopole collision cell, and the quadrupole was set to transmit all ions. Fragmentation of the $[TITLVEVPSDTIENVK + 2H]^{2+}$ ion as well as the $[TLTKG + H]^+$ ion is apparent. The TOF mass spectrum shown on the left was obtained by integrating the two-dimensional data over all drift times. See text for details.

There are a number of prominent peaks in the $[M + H]^+$ family that are not easily assigned. For example, peaks at 6.85(46.15, $m/z = 1359.6$), 6.42(43.90, $m/z = 1230.2$), 5.99(42.16, $m/z = 1131.3$), 5.67(39.68, $m/z = 1002.7$), 5.14(36.94, $m/z = 867.5$), and 4.92(35.19, $m/z = 786.6$) are clearly present, but m/z ratios that are derived are not consistent with tryptic fragments, peptides generated from incomplete digestion, or chymotryptic activity. Additionally, peaks at 4.01(35.22, $m/z = 788.2$) and 3.90(34.69, $m/z = 765.2$) in the $[M + 2H]^{2+}$ family are not easily assigned. Although the source of these features is not clear here, the MS/MS analysis provided below gives a simple means of understanding and assigning these peaks.

Nested Drift(Flight) Time Distributions for All Ions with Gas in the Collision Cell. Figure 4 shows a nested dataset obtained when 3.8×10^{-4} Torr of argon gas is added to the octopole collision cell. In addition to features observed in Figure 3, a prominent series of peaks at 4.44(46.15, $m/z = 1359.6$), 4.44(43.90, $m/z = 1230.2$), 4.44(42.16, $m/z = 1131.3$), 4.44(39.68, $m/z = 1002.7$), and 4.44(37.71, $m/z = 905.2$) is observed. The coincidence in the drift times of these peaks with that of the $[TITLVEVPSDTIENVK + 2H]^{2+}$ ion at 4.44(37.49, $m/z = 894.4$) suggests that the new features arise from fragmentation of this ion. Indeed, the m/z ratios determined from these flight times (1359.6, 1230.2, 1131.3, 1002.7, and 905.2) are in good agreement with calculated values for a series of y-ion fragments⁴⁵ [y_{12} ($m/z = 1359.66$), y_{11} ($m/z = 1230.62$), y_{10} ($m/z = 1131.55$), y_9 ($m/z =$

(45) Fragment nomenclature is consistent with that described by: (a) Biemann, K. *Biomed. Environ. Mass Spectrom.* **1988**, *16*, 99. (b) Biemann, K. *Methods Enzymol.* **1990**, *193*, 886.

1002.51), and y_8 ($m/z = 905.46$)] that would be expected for dissociation of the [TLEVEPSDTIENVK + 2H] $^{2+}$ parent.

The coincidence in drift times can also be used to identify series of other parents and fragments. For example, the [TLTGK + H] $^+$ ion at 3.79(28.64, $m/z = 519.4$) undergoes fragmentation to produce TGG $^+$ (the y_3 ion) at 3.79(22.07, $m/z = 305.2$). In other datasets, we observe very small peaks that can be assigned to fragmentation of other parent ions; under the conditions used to record the data shown in Figure 4, the fragmentation pathways for the majority of [M + H] $^+$ ions are small.

Another feature of Figure 4 is that some peaks that were unassigned in Figure 3 [i.e., 6.85(46.15, $m/z = 1359.6$), 6.42(43.90, $m/z = 1230.2$), 5.99(42.16, $m/z = 1131.3$), 5.67(39.68, $m/z = 1002.7$) in the [M + H] $^+$ family] are clearly apparent and have flight times that are coincident with the y -series fragments [i.e., 4.44(46.15, $m/z = 1359.6$), 4.44(43.90, $m/z = 1230.2$), 4.44(42.16, $m/z = 1131.3$), and 4.44(39.68, $m/z = 1002.7$), respectively] that are produced upon addition of the collision gas. The coincidence in flight times allows the 6.85(46.15, $m/z = 1359.6$), 6.42(43.90, $m/z = 1230.2$), 5.99(42.16, $m/z = 1131.3$), and 5.67(39.68, $m/z = 1002.7$) peaks to be assigned to y -series fragments of [TLEVEPSDTIENVK + 2H] $^{2+}$; these fragments must have been formed during the injection of ions into the drift tube (or during storage in the ion trap).^{29,43} These ions are then separated in the drift tube and fall into the [M + H] $^+$ family, but are not assignable (in Figure 3) because they do not correspond to expected tryptic peptides. The comparison of data obtained with and without gas in the collision cell allows features in the complex dataset, associated with fragments that are formed upon injection into the drift tube (or storage of ions in the trap), to be identified. The case in Figures 3 and 4 allows us to quickly see that the unassigned peaks are due to y -series fragments of [TLEVEPSDTIENVK + 2H] $^{2+}$, formed after ionization, rather than unexpected ionization states of different peptides (such as a metal adduct) or peptides that have undergone post-translational modification.

Nested Drift(Flight) Time Distributions for Selected-Ion Dissociation. Figure 5 shows a nested dataset that is recorded with gas in the collision cell using the quadrupole mass filter to select only $m/z = 894$ (i.e., the [TLEVEPSDTIENVK + 2H] $^{2+}$ parent). The y -series of fragment ions that is observed in this dataset corroborates the assignment of the y -series fragments in Figure 4. Mass selection removes [QLEDGR + H] $^+$, [AKIQDK + H] $^+$, and [LIFAGK + H] $^+$, which have drift times that are near the 4.44 ms value of the $m/z = 894$ parent ion, simplifying the appearance of the two-dimensional dataset.

Collision Cell Pressure Dependence of the Recorded Arrival Time Distributions. An important issue that arises in these studies is the influence of the collision gas pressure upon the ion mobility distributions. The arrival time of ions at the detector is a composite of the drift time (through the He buffer gas), the flight time (in the TOF instrument), and the time required for ions to travel through other portions of the instrument. When the octopole is evacuated, differences between arrival times and drift times are relatively small, ~ 120 to $180 \mu\text{s}$ as compared to the 2–8 ms drift times in these experiments. Addition of a target gas to the octopole collision cell can substantially influence the recorded distributions.

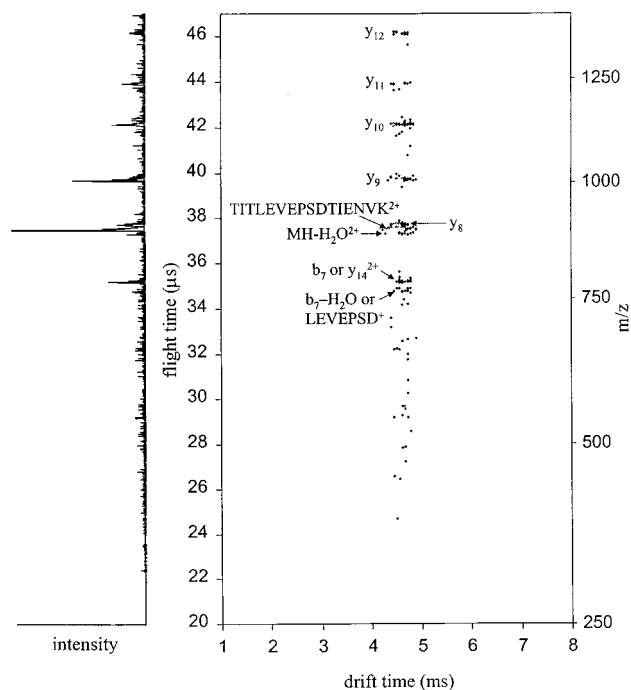


Figure 5. Nested drift(flight) time distribution for the same ubiquitin tryptic mixture as in Figures 3 and 4. Here, the quadrupole was used to select the [TLEVEPSDTIENVK + 2H] $^{2+}$ ion ($m/z = 849$), and 3.8×10^{-4} Torr of argon was added to the octopole collision cell. The TOF mass spectrum shown on the left was obtained by integrating the two-dimensional data over all drift times. See text for details.

Figure 6 shows changes in the arrival time distributions for the $m/z = 531$ and 1061 ions of electrosprayed bradykinin that are observed upon varying the pressure of argon in the collision cell from a background pressure of $\sim 3 \times 10^{-7}$ to 6.0×10^{-4} Torr. These data were recorded by injecting ions into the collision cell using a 30 V potential drop and a 20 V difference between the entrance and exit of the cell. Results for studies conducted over a range of injection voltages (10–60 V) and entrance/exit conditions (biases of 5–50 V), as well as studies of other ion systems, appear similar. The only exceptions are associated with systems that undergo fragmentation to a degree where little or no parent ion signal remains. At ambient background pressures, the arrival time distribution for the $m/z = 531$ ion shows a single sharp peak corresponding to [M + 2H] $^{2+}$. We obtain an experimental resolving power of ~ 30 for this peak. The $m/z = 1061$ slice shows two peaks: a high mobility peak (at ~ 5 ms) corresponding to a doubly protonated dimer, [M $_2$ + 2H] $^{2+}$, and a lower mobility peak (at ~ 6 to 7 ms) that corresponds to the singly protonated monomer, [M + H] $^+$.¹⁰ The experimental resolving powers obtained for the high- and low-mobility peaks are ~ 27 and ~ 23 , respectively. Arrival time distributions recorded at collision cell pressures of 3×10^{-7} to 1×10^{-4} Torr show no reproducible shifts or changes in peak shapes that can be attributed to the addition of the target gas. From simple considerations of the collision cross-sections for these ions (Ω [M + H] $^+$, $\sim 239 \text{ \AA}^2$; Ω [M + 2H] $^{2+}$, $\sim 240 \text{ \AA}^2$; and Ω [M $_2$ + 2H] $^{2+}$, $\sim 378 \text{ \AA}^2$; respectively),¹⁰ target number densities and collision cell path length, we estimate that these ions undergo an average of only one to three collisions at 1×10^{-4} Torr. Ions with smaller collision cross-sections will experience fewer collisions (or use of lower target

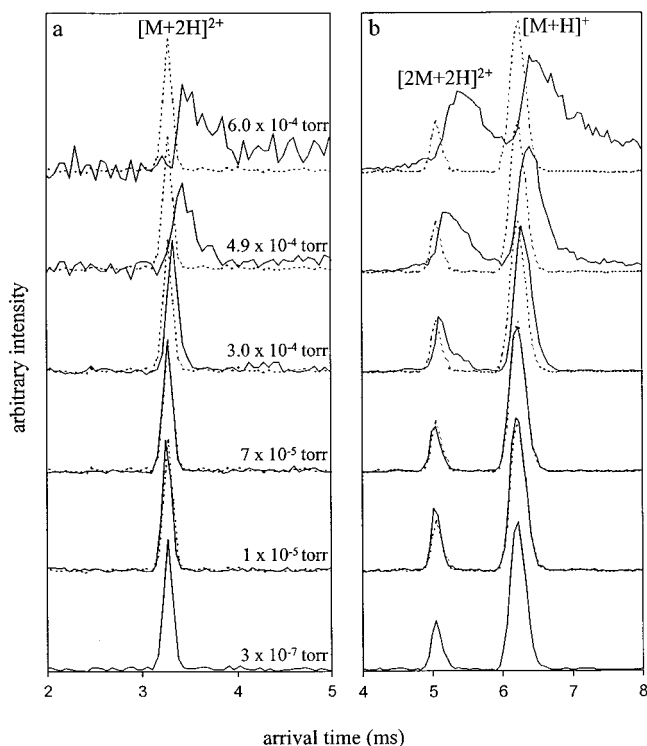


Figure 6. Arrival time distributions for the $m/z = 531$ and 1061 ions of electrosprayed bradykinin observed upon changing the pressure of argon in the collision cell. These data were obtained from nested drift(flight) time distributions by integrating the intensities over specified time-of-flight windows for the drift times shown. Part a shows drift time distributions for the $[M + 2H]^{2+}$ ion of bradykinin at (bottom to top) 3×10^{-7} Torr, 1×10^{-5} Torr, 7×10^{-5} Torr, 3.0×10^{-4} Torr, 4.9×10^{-4} Torr, and 6.0×10^{-4} Torr. Part b shows drift time distributions for the $[M_2 + 2H]^{2+}$ and $[M + H]^+$ ions of bradykinin at the same pressures as in part a. In both cases, the dotted lines correspond to the drift time distributions of the respective ions when the collision cell was evacuated and the base pressure was 3×10^{-7} Torr. The drift window dwell time was $\sim 50 \mu\text{s}$.

pressures in the collision cell). From this, it appears that several collisions do not significantly influence drift time measurement. At higher pressures, peaks are shifted to longer times and are substantially broader than data recorded without target gas. When 3×10^{-4} Torr of gas is added to the collision cell, peaks for all three ions are shifted by $\sim 50 \mu\text{s}$; resolving power estimates obtained from these peaks are similar to those obtained without gas. We estimate that the $\sim 239 \text{ \AA}^2$ $[M + H]^+$ and $\sim 240 \text{ \AA}^2$ $[M + 2H]^{2+}$ ions experience an average of about five collisions and the 378 \AA^2 $[M_2 + 2H]^{2+}$ dimer experiences, eight. These conditions are clearly sufficient to influence the arrival time of the peak; however, the distribution remains reasonably well-defined.

At higher pressures (~ 5 to 6×10^{-4} Torr), the influence of the buffer gas is pronounced. For example, at 4.9×10^{-4} Torr, peaks for all three ions show substantial shifts: $\sim 160 \mu\text{s}$ for $[M + 2H]^{2+}$, $\sim 215 \mu\text{s}$ for $[M_2 + 2H]^{2+}$, and $\sim 160 \mu\text{s}$ for $[M + H]^+$. Measured resolving powers ($t/\Delta t$, where Δt corresponds to the full width at half-maximum of the peak) for these respective peaks are ~ 14 , ~ 12 , and ~ 18 , which are factors of 2.1, 2.3, and 1.3 times below the values obtained without a target gas. Peak shifts and resolving powers for the $[M + 2H]^{2+}$, $[M_2 + 2H]^{2+}$ and $[M + H]^+$ ions recorded at 6.0×10^{-4} Torr are $270 \mu\text{s}$ ($t/\Delta t \sim 7$), $430 \mu\text{s}$ ($t/\Delta t \sim 9$), and $322 \mu\text{s}$ ($t/\Delta t \sim 11$), respectively. At 6.0×10^{-4}

Torr, peaks exhibit substantial tailing at longer times. From analysis of several systems as a function of collision gas pressure, we conclude that in most cases, target pressures of $\sim 8 \times 10^{-5}$ to 4×10^{-4} Torr provide acceptable conditions for generating fragments while maintaining high-quality mobility separations.

SUMMARY AND OUTLOOK

We have shown that ion mobility techniques can be combined with a Q-TOF mass spectrometry configuration to provide an initial separation for a mixture of ions prior to MS/MS analysis. The IMS separation allows ions having similar m/z ratios (but different mobilities) to be isolated and injected into a collision cell for generation of fragmentation patterns and sequence information. This approach should be especially useful for simplifying CID mass spectra obtained for ions having nearly identical m/z ratios. For example, the large differences in mobilities between $[M + H]^+$ and $[M + 2H]^{2+}$ ions having identical m/z ratios would allow the different fragmentation patterns of these ions to be easily distinguished.

An important issue that arises in these studies is the pressure of the target gas in the collision cell. A systematic study of $[M + 2H]^{2+}$, $[M + H]^+$, and $[M_2 + 2H]^{2+}$ ions of bradykinin has been presented in order to illustrate the general constraints of target gas pressure upon mobility measurements and experimental resolving power. The results show that, for the instrumental configuration developed, target gas pressures of $\sim 8 \times 10^{-5}$ to 3×10^{-4} Torr allow ions to undergo sufficient collisions for dissociation without substantial loss of resolving power. Under these conditions, we estimate that this range of ions undergoes ~ 2 to 8 collisions.

Although the IMS-Q/TOF methodology is at a very early stage of development, there appear to be several unique advantages. First, the IMS-MS combination is highly reproducible and selective. When small differences in buffer gas pressure and temperature are taken into account, any two mobility measurements are generally reproducible to within $\pm 1\%$ (relative uncertainty). High-resolution mobility instruments yield higher reproducibility.

Second, as noted above, the use of precursor ion mobilities as labels for fragments generated by CID allows dissociation data to be acquired for mixtures of ions in parallel,⁸ providing a multichannel advantage.⁴⁶ The work presented here was carried out using a low-resolution injected ion drift tube (having a resolving power of ~ 25). With this configuration, the total peak capacity (i.e., the range over which peaks are observed divided by the peak width at the base) is only ~ 10 to 15 for the data shown in Figure 3. A number of groups have developed high-resolution instruments that are capable of resolving powers of more than 200.^{6,47,48} Peak capacities in excess of 100 should be possible with this configuration. An important advantage of the higher resolution IMS separation is that fewer species will have identical mobilities. This will reduce the frequency with which Q selection is required (because many fewer peaks will be unresolved in the mobility dimension).

(46) *Spectrochemical Analysis*; Ingle, J. D., Jr., Crouch, S. R., Eds.; Prentice-Hall: New York, 1988; p 160.

(47) Dugourd, P.; Hudgins, R. R.; Clemmer, D. E.; Jarrold, M. F. *Rev. Sci. Instrum.* **1997**, *119*, 2240.

(48) Wu, C.; Siems, W. F.; Asbury, G. R.; Hill, H. H. *Anal. Chem.* **1998**, *70*, 4929.

Finally, it is interesting to compare unique features of IMS-MS/MS with LC-MS/MS methods which are currently exhibiting extraordinary capabilities for rapid peptide analysis.⁴⁹ A limiting factor associated with LC-MS/MS analysis is that data for an individual component can only be obtained while it is eluting from the column. In this case, analysis would be delayed until a desired species elutes; the gas-phase separation (that takes advantage of high mobilities of ions through a buffer gas) allows mixture complexity to be reduced quickly such that MS/MS can be performed as soon as experiments are initiated. Additionally, LC-MS/MS analysis of very complex mixtures may require that many components be analyzed over short elution times. In this case, the mixture composition changes as components elute from the column. Peak-parking techniques have been developed to extend timeperiods for analysis of complex mixtures.⁵⁰ Because the IMS separation occurs after ionization, the relative amounts of individual components in the mixture remains unchanged during

(49) See, for example: (a) Hunt, D. F.; Yates, J. R., III; Shabanowitz, J.; Winston, S.; Hauer, C. R. *Proc. Natl. Acad. Sci., U.S.A.* **1986**, *83*, 6233. (b) Hunt, D. F.; Michel, H.; Dickinson, T. A.; Shabanowitz, J.; Cox, A. L.; Sakaguchi, K.; Appella, E.; Grey, H. M.; Sette, A. *Science* **1992**, *256*, 1817. (c) Tong, W.; Link, A.; Eng, J. K.; Yates, J. R., III. *Anal. Chem.* **1999**, *71*, 2270. (d) Shevchenko, A.; Jensen, O. N.; Podtelejnikov, A. V.; Sagliocco, F.; Wilm, M.; Vorm, O.; Mortensen, P.; Boucherie H.; Mann, M. *Proc. Natl. Acad. Sci., U.S.A.* **1996**, *93*, 14440. (e) McCormack, A. L.; Schieltz, D. M.; Goode, B.; Yang, S.; Barnes, G.; Drubin, D.; Yates, J. R., III. *Anal. Chem.* **1997**, *69*, 767.

(50) Davis, M. T.; Lee, T. D. *J. Am. Soc. Mass. Spectrom.* **1998**, *9*, 194.

(51) Kulchania, M.; Valentine, S. J.; Srebalus, C. A.; Clemmer, D. E. work in progress.

analysis over indefinite time periods. We expect that upon further development, the ability to examine complex systems for extended time scales will allow low-abundance mixture components to be investigated in detail. This said, we also note that the short time scale required for mobility separation is suitable for coupling with LC.⁵¹ Hill and co-workers have previously developed IMS methods as a rapid detection method for GC and LC.⁵² An instrumental configuration suitable for LC-IMS-MS/MS is currently under construction in our laboratory.

ACKNOWLEDGMENT

The authors are grateful for many helpful conversations regarding instrument development with Dr. Stephen J. Valentine and Dr. Jianwei Li. This work was supported by a grant from the National Institutes of Health (1R01GM-59145-01). We also acknowledge supplemental support of this project from the Camille and Henry Dreyfus foundation. CSH-H gratefully acknowledges generous support from an American Chemical Society Division of Analytical Chemistry Graduate Fellowship sponsored by Merck & Co.

Received for review July 7, 2000. Accepted October 19, 2000.

AC0007783

(52) Wittmer, D.; Chen, Y. H.; Luckenbill, B. K.; Hill, H. H. *Anal. Chem.* **1994**, *66*, 2348.